SAXS Investigations on Relationships between Synthesis Conditions and Solid State Drawability of High Molecular Weight Polyethylene Nascent Reactor Powders. Sintering and Annealing of Powders

Stefano Ottani,[†] Elena Ferracini,[†,‡] Adele Ferrero,[†,‡] Viscardo Malta,[†] and Roger S. Porter*[,§]

Centro di Studio per la Fisica delle Macromolecole del CNR and Dipartimento di Chimica "G. Ciamician", Universitá di Bologna, Via Selmi 2, 40126 Bologna, Italy, and Polymer Science and Engineering Department, University of Massachusetts, Amherst, Massachusetts 01003

Received August 9, 1994; Revised Manuscript Received December 30, 1994[⊗]

ABSTRACT: High and ultrahigh molecular weight polyethylene samples have been investigated by small angle X-ray scattering (SAXS) methods to study the structural changes induced by solid state drawing of nascent reactor powders. The results are correlated with prior reports of differential scanning calorimetry (DSC) and wide angle X-ray scattering (WAXS). The powders were prepared by two different Ziegler–Natta synthesis processes: polymerization in a slurry and in the gas phase. The synthesis temperature range was 30–85 °C. Monoclinic crystals were identified in samples synthesized at 30 °C. SAXS patterns have been recorded at different stages of the solid state processing. Results obtained on nascent reactor powders and on sintered and annealed powder specimens are discussed. No interference peak was ever detected. SAXS profiles obtained from all samples were consistent with the scattering produced by a polydispersed ensemble of particles having approximately globular shape. Values of the radii and of the weight fractions of these gobular aggregates were obtained by Gaussian analysis of their SAXS patterns, according to the iterative generalized Guinier approximation. Results obtained from nascent powders were consistent with five dimensional groups of globular particles. The dependence of weight fractions and globule dimensions on synthesis parameters was investigated. Values of the radii, R_i, of the S185 samples are quasi-multiples of 25 Å, up to the top value of 450 Å of the R_5 group. Such a multiplicity in the sizes of the globular aggregates can be attributed either to the clustering of small subunits into larger particles or to lamellar thickening by preferred doubling during synthesis. Volume contractions of the globular aggregates produced by annealing are more important in samples synthesized at low temperature. Sintering reduces differences among the radii and the weight fractions of different samples. It is proposed that mobility of polymer chain segments is higher for samples synthesized by a slurry process at 85 °C, since modifications induced by sintering and annealing are more important for these samples. Thus the higher chain mobility and the higher ductilies obtained by slurry synthesis at 85 °C suggest that these conditions may lead to nascent powders having lower degrees of entanglement.

Introduction

High and ultra-high molecular weight drawn polymers display higher elasticity as compared to lower molecular weight samples. Such polymeric films and fibers are commonly obtained by extrusion, and by melt or gel spinning techniques. In these methods the specimen undergoes a melt or solubilization step, which obliterates the previous thermal history and provides a more homogeneous material for the subsequent draw. However, these methods cannot be easily applied to polymers of high and ultrahigh molecular weight, because their melt indexes are close to zero and solvent treatments require elevated temperatures and solubilization times, which may affect sample stability. An alternate and successful processing route for these polymers is provided by solid state techniques. In comparison with other methods, like melt or gel spinning, solid state techniques do not require any solvent and allow the use of lower processing temperatures, all below the sample melting point.

One ultimate goal of solid state processing of reactor powders is to draw fibers to extremely high draw ratios to achieve properties, including tensile moduli, as close as possible to the theoretical limit. Solid state methods have proved quite successful when applied to highly ordered systems. Solution grown crystal mats of ultrahigh molecular weight polyethylene (UHMWPE) have been drawn up to 250 times the original length. The final fiber displayed a tensile modulus of 222 GPa, which is very close to the theoretical value reported for a perfect PE crystal.[1] The same method applied to nascent reactor powders proved that these systems are quite ordered and that the drawing process may lead to results similar to those obtained from single crystal mats.[1–5]

Polymer drawing is thought to proceed by extension of an entangled molecular network. The macromolecules are assumed to form a transient network with entanglements acting as friction centers of nonlocalized junctions.[2,6,7] The tensile behavior of a polyolefin fiber can be affected by the extension and the alignment of its chain segments. For low degrees of alignment, deformation at the molecular level is mostly related to torsional rotations of chain segments around the chain backbone. In contrast, with better alignments of chain segments, the mechanical load on the fiber is transferred to the deformation of covalent bonds and bond angles. The force constants of these deformations are higher than the force constants of torsional rotations, and the global elastic response of the polyolefin fiber is

[†] Centro di Studio per la Fisica delle Macromolecole del CNR.
[‡] Dipartimento di Chimica "G. Ciamician".
[§] University of Massachusetts.
[⊗] Abstract published in *Advance ACS Abstracts,* March 1, 1995.

0024-9297/95/2228-2411$09.00/0

improved. Thus, any decrease in the entanglement level should favor drawability, enhancing uniform chain extension and the final mechanical properties of the fiber. This hypothesis was used to discuss the different ductilities of melt-crystallized samples and single crystal mats of PE. Compared to crystallization from dilute solutions, melt crystallization provides conditions more favorable to the formation of entanglements. The much higher drawabilities of single crystal mats of PE would be a direct consequence of less entangled morphologies.[1] This hypothesis also led to the suggestion that nascent reactor powders have lower degrees of entanglements than melt-crystallized morphologies:[2-4] crystallization on synthesis avoids the melting step and the related increase in entanglements. This hypothesis was confirmed for HMWPE nascent reactor powders by investigation of the interphase, the region between the crystal and the amorphous phase, whose volume has been related to the amount of entanglements.[8] The interphase content measured by Raman displays a direct relationship to the maximum achievable draw ratio.[8] Thus, investigations on nascent powder structures can provide an optimal set of synthesis conditions leading to highly ductile polyethylenes.

In the present work, small angle X-ray scattering (SAXS) methods have been used to investigate the structural organization and degree of order of HMWPE reactor powders. Since important structural rearrangements may occur as a consequence of thermal and mechanical treatments, SAXS measurements were carried out for every step of the process in the solid state. Powder specimens are first compacted by compression molding below T_m, the temperature of melting, and subsequently coextruded between the two halves of a split billet of a second polymer. The film coextruded from this assembly can be further drawn to high draw ratios by a tensile force at temperatures just below T_m. The SAXS patterns have been recorded on nascent reactor powders, long time annealed powders (annealed for a maximum of 32 days at two temperatures, 80 and 120 °C), and sintered plates, prepared by pressing reactor powders at temperatures between 120 and 128 °C. At this stage, correlations between structural changes induced by processing and different synthesis conditions can be more easily identified. A second part will be devoted to the analysis of the SAXS patterns of the corresponding coextruded fibers. Comparisons between the undeformed and deformed mesoscopic structures should provide informations on the relationships between synthesis conditions and drawability. In addition to SAXS results, reported and discussed here, these polyethylene samples have been previously tested in several ways and the results obtained by DSC, Raman LAM, WAXS, coextrusion and tensile drawing have already been published.[5,8-11] A short summary of these results is provided here, since it is the background for the discussion of SAXS data.

1. Synthesis. HMWPE samples were synthesized by Union Carbide Corp. (UCC), using Ziegler–Natta heterogeneous catalysis, either by a slurry or gas-phase process.[9] Synthesis temperatures for both processes were 30 and 85 °C. In addition, a temperature of 60 °C was used only in the slurry synthesis. Samples have been classified by the synthesis process type, synthesis temperature, and molecular weight according to the following pattern:

SStt-mm.m

where SS is the synthesis type, tt the synthesis temperature and mm.m the molecular weight. Thus S130-02.9 stands for a sample synthesized by a slurry process at 30 °C, having a molecular weight, $\bar{M}_v$, of 2.9×10^6.

Table 1. Nascent Polyethylene Reactor Powder Characterization

sample identification	$10^{-6}\,\bar{M}_v$[a]	l (Å) DSC[b]	l (Å) Raman LAM[c]	% cryst DSC[d]	hhw DSC[e]	TDR_{max} (135 °C)[f]	tensile modulus (GPa)
HE1900	3.96	284	263	78.9	2.84	104	123
SI30-02.9	2.86	285	284	65.2	2.81	15	
SI30-05.9	5.95	303	299	67.2	2.81	9	
SI30-12.4	12.4	296	304	66.8	2.79	6	
SI30-14.9	14.9	299	296	65.8	2.79	24	
SI60-01.6	1.57	238	258	63.6	2.65	8	
SI85-00.3	0.30	205	218	69.4	2.55	50	49
SI85-00.9	0.93			70.2	2.30		
SI85-01.0	0.96	213	227	67.8	2.30	90	62
SI85-02.0	2.00	211	229	67.6	2.30	85	57
SI85-04.8	4.80	206	225	67.8	2.30	98	75
Gp30-01.9	1.93	277	330	62.4	2.93	7	
Gp85-00.2	0.16	202	240	63.2	3.32	19	
Gp85-01.0	0.96	200	236	64.7	3.32	22	
Gp85-01.2	1.16	192	218	63.0	3.49	9	

[a] Molecular weight viscosity average. [b] Average lamellar thickness, computed by the Thompson–Gibbs equation. [c] Average lamellar thickness, computed by Raman longitudinal acoustic mode. [d] Percent crystallinity computed by DSC enthalpies of melting [e] DSC melting peak width at half-height measured at 0.4 °C/min. [f] Total draw ratio (TDR) is the extrusion draw ratio (EDR) multiplied by the final tensile draw ratio.

Synthesis parameters and polymer characterization are reported in Table 1. Also data on a Hercules HE 1900 sample are reported for comparison.

2. WAXS (Wide Angle X-ray Scattering). WAXS profiles obtained from the nascent powders show the presence of the regular orthorhombic crystals. However, samples synthesized at lower temperatures, 60 and 30 °C, were shown to contain also monoclinic crystals. The amount of the monoclinic phase increases as the synthesis temperature was decreased.[10]

In reactor powders the appearance of monoclinic crystals, sometimes also reported as triclinic, has been often related to deformations of the orthorhombic lattice, arising from the impingement of adjacent growing crystallites during the synthesis (transcrystallization).[12,13]

3. Thermal Analysis. Differential scanning calorimetry (DSC) data obtained from nascent reactor powders provided the following correlations with synthesis parameters.

—Samples synthesized by a slurry process display higher crystallinities. Percent crystallinities were computed from enthalpies of melting, ΔH_m, by the equation:

$$\% \text{ cryst} = \Delta H_m / \Delta H_m^\circ$$

where ΔH_m° (=69.2 cal/g[14]) is the enthalpy of fusion of pure crystalline PE.

—Samples synthesized at lower temperatures display higher melting points. Crystallization and synthesis temperatures are closely related, since the growing polymeric chain crystallizes while it is still involved in the addition of further monomeric units. By using the Thompson–Gibbs equation average lamellar thicknesses, $\bar{l}$, can be computed from the melting temperatures, T_m. Data reported in Table 1 show that lamellar thicknesses are larger for samples synthesized and crystallized at lower temperatures, a result which has been independently confirmed by Raman LAM data.[9,11]

—Nascent reactor powders have average melting temperatures in the range between 134 and 138 °C.[9] However, for most samples the area below the melting peak extends down to temperatures of 90–100 °C. This suggests that thicknesses of nascent crystallites are distributed over a broad dimensional range. The crystallite size distribution was estimated by the melting peak width at half-height (hhw in Table 1). DSC scans at 0.4 °C/min showed that samples synthesized at 85 °C by a slurry process have lower hhw values. It was concluded that these synthesis conditions lead to narrower crystallite size distributions.

4. Coextrusion and Second Stage Draw. Reactor powders were compacted at 120 °C into thin plates that were subsequently cut into small strips. These strips were inserted between the two halves of a high-density polyethylene split cylindrical billet. The sealed billets were coextruded at 120 °C through a conical bronze die. Dimensions of the die were appropriately chosen to obtain an extruded draw ratio (EDR) of about 8. The coextruded fibers were subsequently drawn at 135 °C to the maximum achievable extension. Values of the maximum total draw ratio (TDR_{max}) were computed as the product of EDR by the tensile draw ratio. The results are summarized in Table 1.[5,9]

This table indicates that samples synthesized at 85 °C by a slurry process show higher values of TDR_{max}, and the corresponding tensile moduli are higher. It is also evident that only this particular combination of synthesis parameters leads to most ductile polyethylene reactor powders. Thus, synthesis conditions can be thought of having a close control over sample ductility and ultimate tensile properties.

5. Crystallinity and Drawability. On seeking the structural parameters controlling the sample ductility, an assumption has been made, based on the entanglement model for chain dynamics,[15] that lower levels of entanglement would lead to higher attainable TDR_{max}. As reported in the Introduction, this hypothesis led also the suggestion that nascent reactor powders have less entanglements than melt-crystallized morphologies,[2–4] since they are crystallized directly on synthesis, avoiding the increase in entanglements which may take place in the molten state. The higher crystallinities of nascent powders, as compared to melt-crystallized samples,[9] may provide experimental support to this hypothesis.

On crystallization and annealing, entanglements and tie molecules are preferentially rejected from the crystalline body, so that they mostly concentrate in the interlamellar layers.[16] In fact highly entangled systems cannot easily provide the long-range three-dimensional order required to develop both thick lamellar crystals and high degrees of crystallinity. Thus percent crystallinity may provide a good estimate of the degree of order of semicrystalline polymeric systems and also an indirect estimate of the overall degree of entanglements. A semilogarithmic plot of the percent crystallinity of the nascent reactor powders *vs* TDR_{max}, as reported in Figure 1, displays a reasonable correlation. However, such a correlation is insensitive. Figure 1 shows that TDR_{max} increases almost 1 order of magnitude as percent crystallinity is increased from only 67.2 to 67.6. Albeit, the above described model provides a correlation between crystallinity and drawability, it is based on a simplified picture of the molecular arrangements which can influence ductility. In fact, for samples crystallized

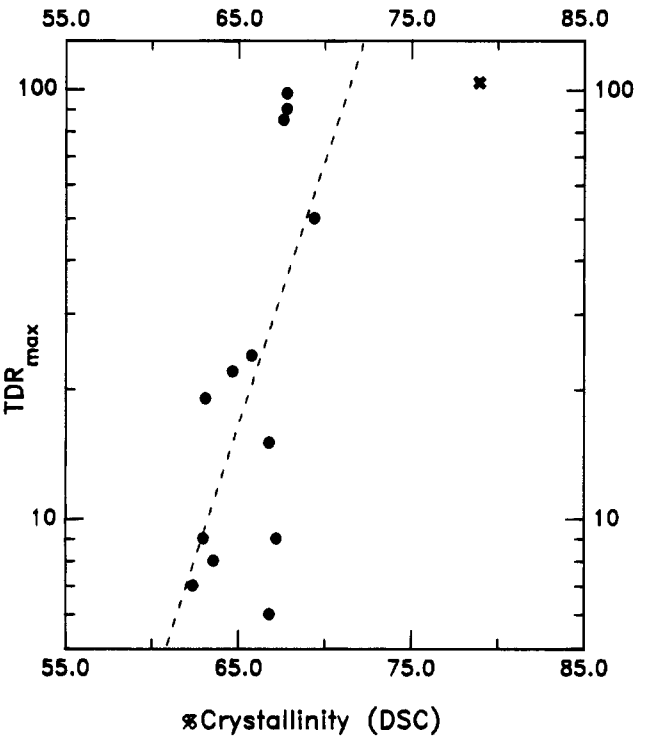

Figure 1. Nascent polyethylene percent crystallinity *vs* maximum total draw ratio: (●) UCC samples; (×) HE1900; (dashed line) least squares fit to UCC samples.

directly on synthesis the effects of high undercoolings on the crystallization dynamics must be considered.[17–20] The degree of order of the crystallite fold surfaces is related to the crystallization regime.[18] More disordered surfaces can increase the displacement of chain segments from their crystallographic positions and can transmit such displacements more deeply into the crystallite cores. Thus, a slight reduction in crystallinity can be expected for crystallization at high undercoolings.

In the above section on thermal analysis it was reported that crystallinity is controlled by synthesis conditions. Table 1 shows that for a given synthesis process, gas-phase, or slurry, crystallinities decrease as the undercooling for synthesis is increased. Thus the same set of conditions leading to higher crystallinities should produce more highly drawable samples. Data in Table 1 show that the best combination of synthesis conditions is given by a slurry process at 85 °C.

6. RAMAN Spectroscopy. The significance of the correlation between TDR_{max} and nascent percent crystallinity is confirmed by Raman spectroscopy on nascent powders.[8] Results obtained by Raman investigations on semicrystalline polymers can be interpreted on the basis of a model proposed by Strobl and Hagedorn.[21] According to this model, chain segments in a polycrystalline material can be subdivided in three classes: crystalline, amorphous, and segments belonging to the interphase. This last class represents a disordered phase of anisotropic nature, located in a transition zone between crystalline and amorphous regions. The anisotropic character of this interphase arises from partial orientation of stretched chain segments which, however, lack lateral order. Entanglements are presumed to concentrate in the interphase. Thus chain slippage in this region may control the overall drawability, by limiting both the deformation of the interlamellar layers and the mobility of the crystallographic planes.

Results obtained by Raman spectroscopy on nascent reactor powders are of great importance. In fact, data

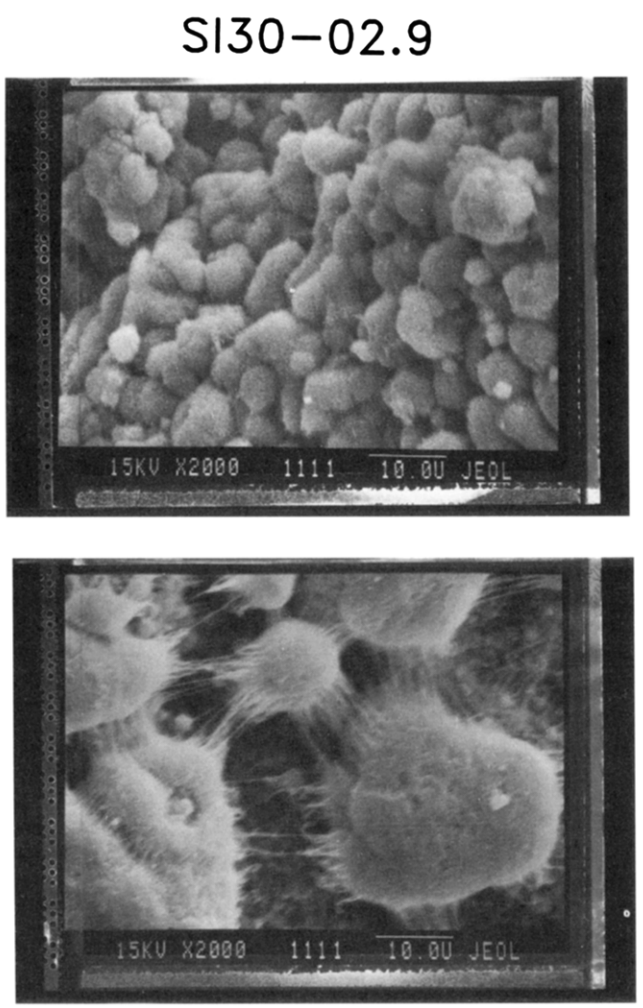

Figure 2. (a) SEM photograph of the S130-02.9 nascent reactor powder. The 10.0U white bar at the bottom corresponds to 10.0 μm. (b) SEM photograph of the S185-04.8 nascent reactor powder.

prove that a lower interfacial content correlates well with higher drawability.[8] Moreover, Raman and DSC crystallinities are in good agreement, which provides strong experimental evidence concerning relations among chain entanglements, nascent crystallinity, sample ductility, and synthesis parameters.

7. Scanning Electron Microscopy. Investigations on morphologies of nascent reactor powders have been carried on by scanning electron microscopy (SEM). Parts a and b of Figure 2 report typical morphologies corresponding to different synthesis conditions. Samples synthesized at higher temperatures (85 °C) show looser globular packing (cobweb-like structures) as compared to the more compact aggregates obtained by synthesizing at lower temperatures. Clustering of small single globular particles of polymer seems to be a characteristic feature of nascent specimens obtained by high-yield Ziegler–Natta catalysts.[22–25] X-ray microtomography[22,23] and image analysis of SEM photograms[26,27] have led to the conclusion that the size and shape of these globular aggregates are related to the size and the activity of the catalyst particles and to the fragmentation of the catalyst support during polymerization.

Both types of aggregates in Figure 2a,b have been described[24] as obtained from aggregation of smaller subunits. A higher synthesis temperature may induce some swelling of the nascent clusters; separation of individual globules will then leave some thin filaments among the particles which provide the characteristic cobweb arrangement. In contrast, the closer packing of globules in Figure 2a suggests that transcrystallization may occur as a consequence of the lateral impingement of growing polymer particles. This conclusion is in agreement with the presence of monoclinic crystals in the samples synthesized at 30 °C.[12,13]

Experimental Section

SAXS measurements were performed on HMWPE samples obtained after every step of the solid state drawing procedure. The following specimens were investigated.

(a) *Nascent reactor powders* as obtained by synthesis, without any further treatment. At this stage all samples reported in Table 1 were examined to investigate possible structural differences induced by synthesis conditions.

(b) *Sintered plates* were prepared by pressing reactor powders at 150 kg cm^{-2} under vacuum for about 8 h. Plate thickness was 1 mm and processing temperatures ranged between 120 and 128 °C, which is about 10–15 °C below the DSC melting peak temperature.

(c) *Reactor powders annealed at different temperatures* below the melting point. Powder specimens were placed in glass vials which were sealed after air evacuation. Vials were introduced in two oil baths at 80 and 120 ± 1 °C. All samples were annealed for 32 days. In addition another set of samples was annealed at 80 °C for only 15 days. Long annealed powders were prepared with the purpose of enhancing structural changes stemming from the monoclinic to orthorhombic phase transition. This crystal conversion takes place at temperatures close to 80 °C. At this low temperature other annealing effects can be neglected. Comparisons with samples annealed at 120 °C may provide a method to isolate effects stemming from the monoclinic–orthorhombic phase transition.

(a), (b), and (c) samples have been investigated by a high-resolution Kratky camera (Compact) with Cu Kα radiation. Intensities were recorded by a proportional counter with pulse height discriminator. Data were collected at b values ($|b| = b = 2(\sin\vartheta)/\lambda$) ranging from 9.5×10^{-4} to 4.5×10^{-2} Å^{-1}. Slit widths for all the scans were 80 μm for the entrance slit and 200 μm for the counter slit. Desmearing of recorded intensities was performed according to the procedure reported by Vonk.[28]

Results and Discussion

1. Reactor Powders. The most remarkable difference among SAXS profiles recorded from nascent reactor powders and the SAXS patterns usually obtained from melt-crystallized PE samples[29–31] is the absence of any interference peak (Figure 3). Thus, in nascent reactor powders no evidence is obtained of a long spacing, which is the most distinctive characteristic of a regular lamellar organization. Since similar profiles were obtained from all (a) samples, the stacking of crystalline lamellae in these reactor powders must be highly irregular.[32,33] It can also be noted that lamellar arrangement in nascent reactor powders seems to depend on the catalyst. In fact, in the case of polypropylene, a long period can be measured in SAXS patterns obtained from nascent reactor powders synthesized by conventional Ziegler–Natta catalysts.[34] In contrast, this feature is not present in nascent isotactic polypropylene polymerized by a high-yield heterogeneous Ziegler–Natta catalyst supported on $MgCl_2$.[34] However, in this last case, the presence of intensity fluctuations in the SAXS profiles was found to be compatible with the scattering patterns of aggregates of dimensionally monodispersed spherical globules.

As reported in Figure 3, the HMWPE nascent powder patterns do not show any intensity fluctuations stem-

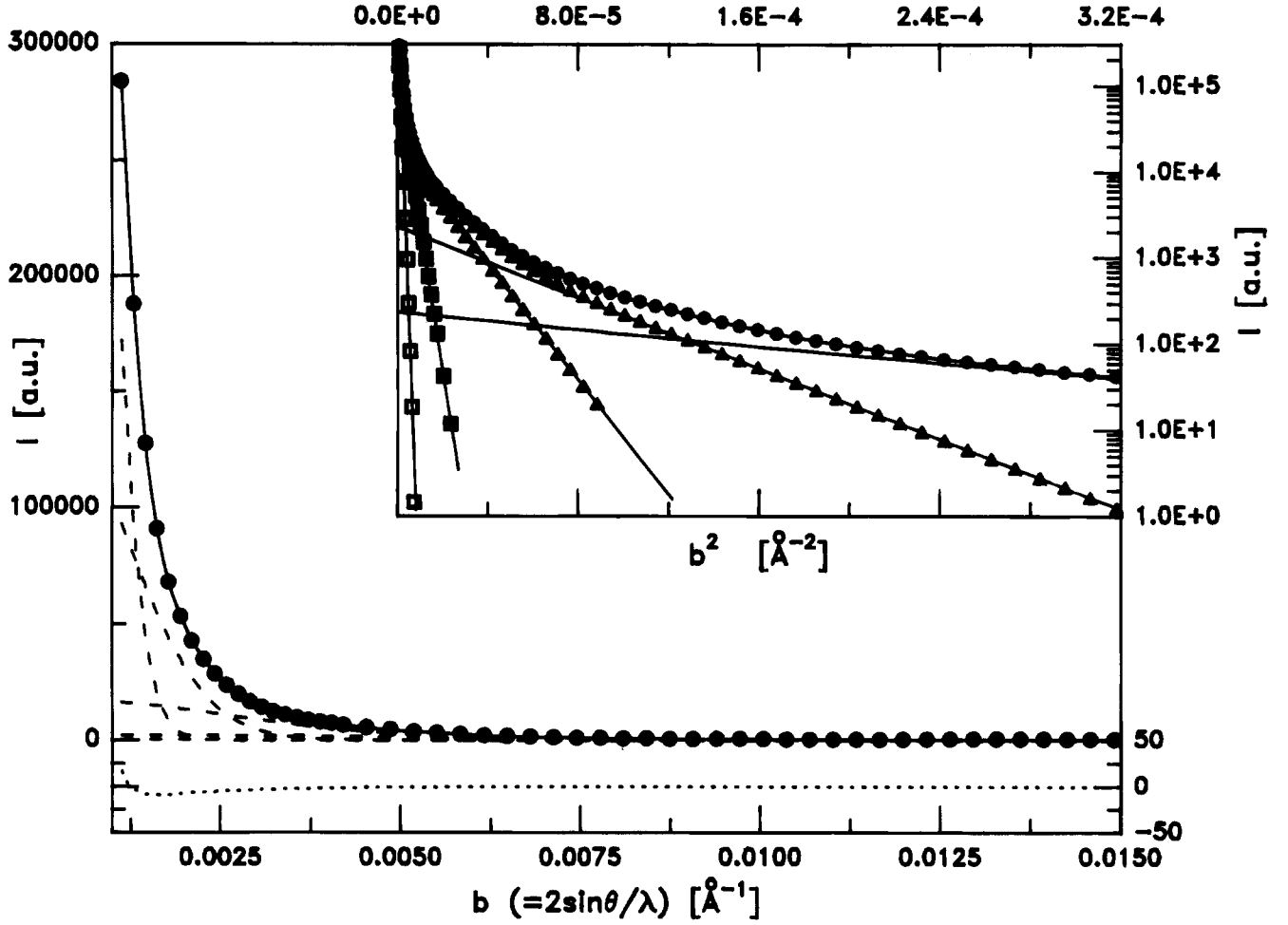

Figure 3. Guinier analysis of the SAXS profile of the S185-02.0 nascent reactor powder. (●) experimental points; (—) least squares fit; (- - -) individual Gaussian components of the least squares fit; (···) difference curve (=experimental − least squares fit). To enhance visibility, the *y*-scale of the difference curve has been enlarged. On the top-right corner the same results are reported in terms of the well-known Guinier plot.

ming from the scattering of monodispersed particles of a defined shape. The simultaneous absence of interferential peaks and of intensity fluctuations suggest that scattering in these nascent systems should be rather ascribed to a polydispersed ensemble of particles having approximately globular shapes. It has been reported that, if the polydispersity of globule dimensions is larger than their packing density, the SAXS profiles of such systems follow the pattern of the Guinier regime in its Gaussian approximation.[35-37] Conditions for scattering in the Guinier regime are normally fulfilled by dilute systems, where interparticle interference is absent. Albeit in reactor powders interparticle interference cannot be completely excluded, its typical effect, *viz.* the dropping of intensities scattered at very low angles,[38] was not detected in the SAXS profiles recorded on (a), (b), and (c) samples. In these conditions the scattering of the whole system is satisfactorily described as just the sum of the scattering from the single particles.[39]

Analysis of the SAXS patterns was performed by nonlinear least squares methods, fitting a model function with adjustable parameters to the desmeared profiles. The model function was made up by a summation of Gaussian functions (the Guinier components) plus a constant background to account for the liquid-like scattering superimposed on the SAXS patterns of many samples.[40] The iterative application of the generalized Guinier method provided the initial guess for the set of Gaussian functions:

$$I_i(b) = I_i(0) \exp\left(-\frac{4}{3}\pi^2 b^2 R_{gi}^2\right) \quad (1)$$

where R_{gi} is the electronic radius of gyration of the ith dimensional group of spherical particles. The corresponding spherical radius is given by $R = R_g(5/3)^{1/2}$. The Gaussian function in eq 1 is the Guinier approximation to the component scattering of a polydisperse system and is obtained by truncation of the power series which describes the scattering intensity of the ith group of particles.[41] Values of R_{gi}, $I_i(0)$, and of the background were adjusted by nonlinear least squares to obtain the best fit to the desmeared SAXS profile. Figure 3 reports the typical outcome of this global fitting and the individual contributions of the dimensional groups to the total scattering. The weight distribution function, $W(R)$, of the globular particles is related to the scattered intensities by the following equation:[41]

$$I(b) = C\int_0^\infty W(R)\, R^3 \exp\left(-\frac{4}{3}\pi^2 b^2 R_g^2\right) dR \quad (2)$$

where C is a constant. For a finite number of groups the integral in eq 2 can be replaced by a sum. Extrapolation of intensities to $b = 0$ gives

$$I(0) = C\sum_i W_i(R_i)\, R_i^3 \quad (3)$$

Table 2. Polyethylene Nascent Reactor Powders: X-ray Guinier Analysis Results

Average Particle Radii of Distinguishable Dimensional Groups

sample identification	$10^{-6}\bar{M}_v$	R_1[Å]	R_2[Å]	R_3[Å]	R_4[Å]	R_5[Å]
HE1900	3.96		30	66	141	343
SI30-02.9	2.86	29	61	117	240	469
SI30-05.9	5.95	23	36	67	138	328
SI30-12.4	12.4	24	36	64	133	323
SI30-14.9	14.9		33	67	139	331
SI60-01.6	1.57	29	48	68	133	317
SI85-00.3	0.30	27	54	98	227	453
SI85-00.9	0.93	28	55	99	229	457
SI85-01.0	0.96	27	52	96	231	462
SI85-02.0	2.00	28	55	99	224	456
SI85-04.8	4.80	34	69	111	231	466
Gp30-01.9	1.93	27	32	66	142	331
Gp85-00.2	0.16	25	42	75	136	323
Gp85-01.0	0.96	26	41	74	132	326
Gp85-01.2	1.16	24	40	73	132	314

Average Mass Fractions of Dimensional Groups R_i

sample identification	$10^{-6}\bar{M}_v$	wt % (R_1)	wt % (R_2)	wt % (R_3)	wt % (R_4)	wt % (R_5)
HE1900	3.96		13	18	25	44
SI30-02.9	2.86	14	19	17	18	32
SI30-05.9	5.95	8	12	21	23	36
SI30-12.4	12.4	10	12	24	22	32
SI30-14.9	14.9		19	25	23	33
SI60-01.6	1.57	11	5	17	29	38
SI85-00.3	0.30	15	20	27	18	19
SI85-00.9	0.93	16	22	26	17	18
SI85-01.0	0.96	15	20	27	17	20
SI85-02.0	2.00	15	19	26	19	21
SI85-04.8	4.80	18	22	18	18	24
Gp30-01.9	1.93	5	11	20	24	40
Gp85-00.2	0.16	11	12	22	17	37
Gp85-01.0	0.96	12	11	24	17	36
Gp85-01.2	1.16	11	11	22	19	37

Equation 3 can be combined with the values of $I_i(0)$ and R_i obtained by least squares to compute the weight fractions, wt % (R_i), corresponding to that portion of globules of average radius $\bar{R} = R_i$. Weight fractions have been evaluated under the assumption that the complete set of dimensional groups in the specimen can be identified in the experimental b range used to record the SAXS pattern. This does not completely exclude the presence of larger globules, since their contribution to SAXS intensities could be detected only by extending measurements to smaller angles. It must be pointed out that the accuracy of the parameters of the largest dimensional group is slightly lower, because only a restricted number of experimental points is available to compute this contribution.

Results of Guinier analysis on nascent powders are reported in Table 2. These results are consistent with a maximum of five dimensional groups. Average radii, R_i, and the corresponding mass fractions, wt % (R_i), of these groups are reported. R_i values of globular particles range in the interval 25–450 Å. This broad dimensional interval is also consistent with previous estimates of the crystallite size distribution by DSC (see the hhw values in Table 1).[9] Moreover, DSC scans at 0.4 °C/min showed that at 90–100 °C small amounts of the nascent crystallites have already melted. These thin and less stable crystallites can actually be a component of the smallest dimensional groups listed in Table 2. These data confirm that the global polydispersity is sufficiently high to satisfy the condition previously mentioned of globule polydispersity larger than packing density.

The Guinier method seems particularly fit for the analysis of the nascent globular structures commonly found in polyolefin samples obtained by Ziegler–Natta catalysts.[24–27,34] Previous studies on the structure and morphology of these globular systems showed that they can be obtained by aggregation of smaller subunits, which pack differently, depending on the polymerization conditions.[24] On synthesis, the growing of complex aggregates in the shape of ribbons or cobwebs has been attributed to the coalescence of smaller polymer globules surrounding a catalyst fragment.[24,25] SAXS and WAXS investigations on these subunits led to the conclusion that large globules are made up by macroaggregates of microparacrystals, with binding forces provided by the microparacrystal surface free energies.[34] Values of R_i in Table 2 may confirm the existence of such multiglobular aggregates. In fact some degree of multiplicity is detected on passing from the smallest to the largest dimensions. This is especially evident for the S185 samples whose values of R_i are quasi-multiples of 25 Å. For these samples, the diameter of a particle of the second group corresponds to the sum of the diameters of two particles of the first group. This summation can be extended up to the diameter of the largest group, supporting the hypothesis that at least part of the bigger aggregates have been obtained by coalescence of small subunits.

However, a different explanation can be proposed. Observations of the preferred doubling of the initial fold length have been reported for the annealing of several polymers.[42] According to such observations, thickening of crystalline lamellae would proceed by fold dislocation, doubling and eventually quadrupling the initial fold length. Synthesis conditions can actually favor crystallite thickening by annealing. Crystallization during polymerization follows different paths depending on the synthesis temperature.[20,43] At low temperatures polymerization and crystallization rates are quite close and a simultaneous polymerization–crystallization mechanism is favored. In contrast, at higher temperatures, above 70 °C for PE, polymerization and crystallization proceed separately; annealing becomes important and influences the final crystallinity.[9,20] Both the multiglobular clusters and the crystallites thickened by preferred doubling are consistent with results reported in Table 2. However, beyond the results of the Gaussian analysis further information is required to decide which model better describes the inner structure of the globular aggregates.

These observations are also useful to compare dimensions of the globular aggregates with the average lamellar thicknesses reported in Table 1. S185 samples display values of l of about 200 Å, suggesting that crystallites of this size can be part of the globules of the third and higher dimensional groups. Globule diameters of about 200 Å (the third group) and 460 Å (the fourth group) are well compatible with the thicknesses of one or two crystallites, respectively, while more complex arrangements are required to account for the dimensions of the fifth group. This same compatibility is observed for the two largest groups of the S130 and Gp samples. Thus, according to these observations, the largest globules would be made up by clusters of crystallites whose thickness is a function of the synthesis temperature. It can be noted that this assumption agrees with the dependence of $\bar{l}$ on the synthesis temperature, as discussed in the previous section on thermal analysis.[11] However, direct experimental sup-

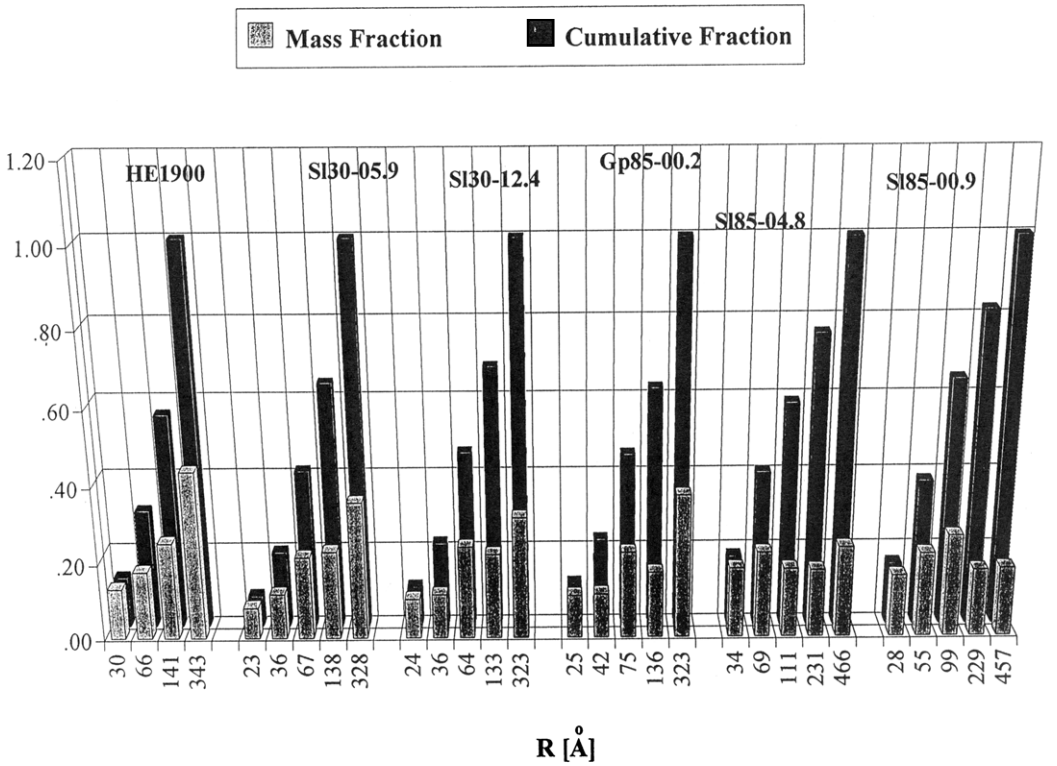

Figure 4. Effects of synthesis conditions on the cumulative fractions and the mass fractions of dimensional groups of nascent reactor powders. Values of the corresponding Guinier radii are reported as abscissae.

port for this assumption can only be only provided by further investigations on the inner structure of the globular aggregates.

Several attempts to analyze the SAXS patterns by the Vonk method[44] did not provide reliable results. Application of the Porod law to the tail portions of the scattering curves resulted in values of the interphase layer thicknesses close to zero. This result agrees with the globular character of the nascent powder specimens: the high intensities scattered by loosely packed nascent aggregates are consistent with large amounts of microvoids among the powder grains (see also Figure 2). Thus the electron density falls rapidly to zero at the globule surface, obliterating the smaller fluctuations stemming from the crystal–amorphous interface. Moreover, oscillations in the tail data, often leading to negative values of the interphase layer thicknesses, do not allow precise evaluations of the background contribution to the total scattering. This greatly reduces the reliability of computations of the particle size distribution function.[44] Under these conditions, estimating the number of crystallites or smaller units which may be part of the larger globules is a problem beyond the resolving power of the method applied in this study. A structural model to perform a global fitting of the scattering profiles is likely required, but such a procedure is beyond the scope of the present work.

Inspection of data in Table 2 and Figure 4 shows that the well-defined multiplicity in the R_i values of the S185 samples is less evident in samples synthesized in different conditions. S130 samples still display some degree of multiplicity in the larger dimensional groups, while relationships among R_i values of the Gp85 samples are much more irregular. The cumulative fractions reported in Table 2 and Figure 4 show a slight dependence of mass distribution on synthesis parameters. Slurry synthesis at 85 °C increases dimensions of the smaller groups. At the same time larger amounts of polymer are aggregated into particles with diameters >100 Å. Moreover, wt % (R_5) of the S185 samples is smaller than the corresponding fractions of the largest dimensional group of the other samples. Thus, synthesis of 85 °C in slurry favors midsize globular aggregates, while more unbalanced mass distributions are obtained with different synthesis conditions. An analogous correlation between crystallite size distributions and synthesis conditions has been obtained by the hhw values of DSC melting peaks (Table 1).[9] As a final remark, no definite correlation was found between $\bar{M}_v$ and particle radii.

2. Sintered and Annealed Powder Samples. SAXS measurements were performed on sintered and annealed powders to investigate structural changes induced by the first step in the solid state drawing procedure. Samples of types (b) and (c) were selected for testing as representative of different sets of synthesis conditions. SAXS patterns were similar to those previously recorded from nascent reactor powders. As reported in Figure 5, no long period interference peak was detected and average radii and mass fractions of globular particles were obtained by the Gaussian method, as described previously. Figure 5 shows also that some small fluctuations in the scattered intensities can be observed at larger angles. This might be attributed to the presence of a monodisperse particle, which could have been produced by some crystallite reorganization on annealing and sintering. However, quantitative attempts to analyze such oscillations did not provide any consistent result. Globular particles in sintered specimens are more packed than in nascent powders, so that effects of interparticle interference cannot be completely excluded. Validity of the SAXS profile analysis by the Guinier method of sintered samples is actually based on the indirect evidence that in annealed and sintered samples interparticle interference is still negligible. This indirect evidence is essentially provided by (i) the lack

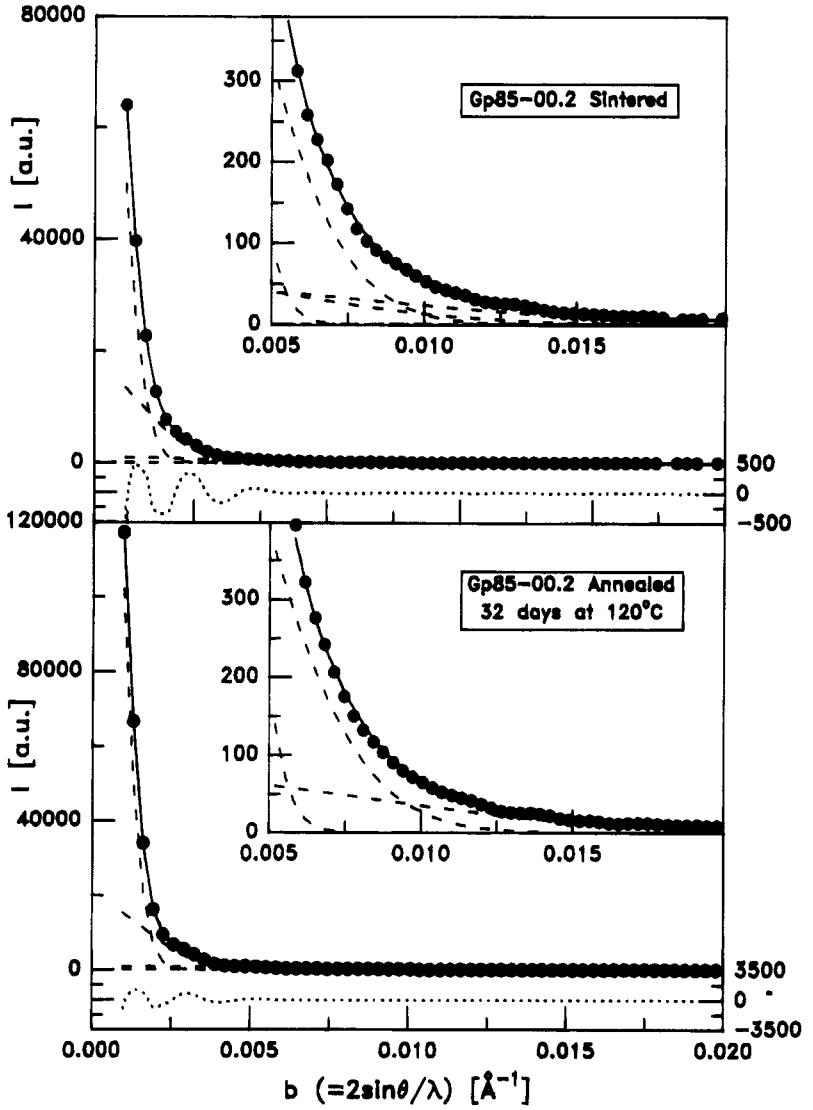

Figure 5. Typical results of the Guinier analysis on sintered and annealed samples. Symbols and line types as in Figure 3. Enlarged views of the tail portions of the SAXS profiles are plotted on the top-right corners of each graph.

of any intensity drop in the initial portions of the SAXS profiles, (ii) the similarity between patterns obtained from sintered specimens and annealed powders which were not compacted, and (iii) and high global polydispersity in systems of five dimensional groups with remarkably different values of their radii.

Tables 3 and 4 report R_i values and mass fractions of annealed samples and sintered plates. Sintering at high temperatures in simultaneously a mechanical and thermal process. In contrast annealed samples have only undergone a thermal treatment. Comparisons between these two types of samples should allow separation of the thermal and the mechanical effects. Comparative pictures of the changes in particle polydispersity are reported in Figure 6. Polydispersity is reduced and the average size of largest globules is increased, which confirms that the global effect of annealing and sintering at high temperatures is to improve the degree of order in the system.

Structural changes induced by annealing of single crystals and melt-crystallized samples have been widely investigated and correlated with annealing temperature.[45] Three temperature regions have been identified:

(i) Low-temperature region, where changes are restricted to a decrease in defect concentration and stress relief.

(ii) Intermediate-temperature region, where increases in chain fold length and in crystal size can be detected, both processes taking place without melting.

(iii) High-temperature region, where partial melting (melting of less perfect crystallites) and recrystallization is the dominant process. Most of the mass transfer on annealing takes place in this temperature region.

Studies on polyethylene single crystal mats provided well-defined temperature boundaries for these three regions (between 118 and 123 °C for the intermediate-temperature region).[45] In contrast, melt-crystallized samples do not display such sharp temperature boundaries. Difficulties with these samples stem from the evaluation of defects within and between crystal lamellae, which provide the major contribution to the state of stress at lower temperatures. Nevertheless, the large amount of data reported on polyethylene[45] leads to the conclusion that the annealing of single crystal mats and melt-crystallized samples produces effects which can be unambiguously related to a specific temperature region.

Application of the three-step model, above, to the annealing of reactor powders does not provide the same reliable correlations. For crystallization on synthesis at 30 and 85 °C, the high undercooling and the large temperature gradients at the catalyst surface lead to a broad collection of crystallite dimensions (Table 2 and

Table 3. Polyethylene Reactor Powders: Average Particle Radii and Average Mass Fractions of Dimensional Groups R_i, for Different Annealing Conditions

Sample HE1900

annealing temp (°C) and time (days)	R_1[Å]	R_2[Å]	R_3[Å]	R_4[Å]	R_5[Å]	annealing temp (°C) and time (days)	R_1[Å]	R_2[Å]	R_3[Å]	R_4[Å]	R_5[Å]
nascent powder		30	66	141	343	80, 32		29	59	126	316
80, 15		27	56	124	313	120, 32		30	64	151	357
annealing temp (°C) and time (days)	wt % (R_1)	wt % (R_2)	wt % (R_3)	wt % (R_4)	wt % (R_5)	annealing temp (°C) and time (days)	wt % (R_1)	wt % (R_2)	wt % (R_3)	wt % (R_4)	wt % (R_5)
nascent powder		13	18	25	44	80, 32		12	16	24	48
80, 15		12	16	25	48	120, 32		10	16	27	47

Sample SI30-14.9

annealing temp (°C) and time (days)	R_1[Å]	R_2[Å]	R_3[Å]	R_4[Å]	R_5[Å]	annealing temp (°C) and time (days)	R_1[Å]	R_2[Å]	R_3[Å]	R_4[Å]	R_5[Å]
nascent powder		33	67	139	331	80, 32		29	59	126	300
80, 15		30	58	115	283	120, 32	26	36	70	150	330
annealing temp (°C) and time (days)	wt % (R_1)	wt % (R_2)	wt % (R_3)	wt % (R_4)	wt % (R_5)	annealing temp (°C) and time (days)	wt % (R_1)	wt % (R_2)	wt % (R_3)	wt % (R_4)	wt % (R_5)
nascent powder		19	25	23	33	80, 32		15	20	28	37
80, 15		23	22	32	23	120, 32	5	10	18	29	38

Sample SI60-01.6

annealing temp (°C) and time (days)	R_1[Å]	R_2[Å]	R_3[Å]	R_4[Å]	R_5[Å]	annealing temp (°C) and time (days)	R_1[Å]	R_2[Å]	R_3[Å]	R_4[Å]	R_5[Å]
nascent powder	29	48	68	133	317	80, 32	28		53	115	275
80, 15	26		52	114	273	120, 32	32		71	156	334
annealing temp (°C) and time (days)	wt % (R_1)	wt % (R_2)	wt % (R_3)	wt % (R_4)	wt % (R_5)	annealing temp (°C) and time (days)	wt % (R_1)	wt % (R_2)	wt % (R_3)	wt % (R_4)	wt % (R_5)
nascent powder	11	5	17	29	38	80, 32	11		15	31	43
80, 15	12		16	31	41	120, 32	12		16	32	40

Sample SI85-04.8

annealing temp (°C) and time (days)	R_1[Å]	R_2[Å]	R_3[Å]	R_4[Å]	R_5[Å]	annealing temp (°C) and time (days)	R_1[Å]	R_2[Å]	R_3[Å]	R_4[Å]	R_5[Å]
nascent powder	34	69	111	231	466	80, 32	26	50	98	268	
80, 15	27	49	97	267		120, 32	44	82	150	333	
annealing temp (°C) and time (days)	wt % (R_1)	wt % (R_2)	wt % (R_3)	wt % (R_4)	wt % (R_5)	annealing temp (°C) and time (days)	wt % (R_1)	wt % (R_2)	wt % (R_3)	wt % (R_4)	wt % (R_5)
nascent powder	18	22	18	18	24	80, 32	15	21	33	31	
80, 15	15	20	33	32		120, 32	24	17	30	29	

Sample Gp30-01.9

annealing temp (°C) and time (days)	R_1[Å]	R_2[Å]	R_3[Å]	R_4[Å]	R_5[Å]	annealing temp (°C) and time (days)	R_1[Å]	R_2[Å]	R_3[Å]	R_4[Å]	R_5[Å]
nascent powder	27	32	66	142	331	80, 32	27		56	121	292
80, 15	23		52	117	286	120, 32		31	68	152	335
annealing temp (°C) and time (days)	wt % (R_1)	wt % (R_2)	wt % (R_3)	wt % (R_4)	wt % (R_5)	annealing temp (°C) and time (days)	wt % (R_1)	wt % (R_2)	wt % (R_3)	wt % (R_4)	wt % (R_5)
nascent powder	5	11	20	24	40	80, 32	13		17	28	42
80, 15	13		17	28	42	120, 32		14	17	29	40

Sample Gp85-00.2

annealing temp (°C) and time (days)	R_1[Å]	R_2[Å]	R_3[Å]	R_4[Å]	R_5[Å]	annealing temp (°C) and time (days)	R_1[Å]	R_2[Å]	R_3[Å]	R_4[Å]	R_5[Å]
nascent powder	25	42	75	136	323	80, 32	27		53	107	296
80, 15	28		54	106	295	120, 32	31		67	151	346
annealing temp (°C) and time (days)	wt % (R_1)	wt % (R_2)	wt % (R_3)	wt % (R_4)	wt % (R_5)	annealing temp (°C) and time (days)	wt % (R_1)	wt % (R_2)	wt % (R_3)	wt % (R_4)	wt % (R_5)
nascent powder	11	12	23	17	37	80, 32	14		17	29	40
80, 15	15		17	29	39	120, 32	15		18	31	36

Table 4. Particle Dimensions and Average Mass Fractions after Sintering

sample identification	sintering temp (°C)	R_1[Å]	R_2[Å]	R_3[Å]	R_4[Å]	R_5[Å]
SI30-05.9	128	30	48	76	153	315
SI30-12.4	122	33		70	151	320
SI85-02.0	127	33	56	87	167	322
Gp85-01.0	120	31	65		140	347
Gp85-00.2	124	30	44	74	159	330

sample identification	sintering temp (°C)	wt % (R_1)	wt % (R_2)	wt % (R_3)	wt % (R_4)	wt % (R_5)
SI30-05.9	128	14	7	20	27	32
SI30-12.4	122	19		24	28	29
SI85-02.0	127	18	12	18	28	24
Gp85-01.0	120	19	24		35	22
Gp85-00.2	124	14	6	20	34	26

ref 9). For these reactor powders an annealing temperature of 80 °C may fall in the high temperature region (iii), instead of being within the first region, as normal for melt or solution-crystallized polyethylene. Moreover, the shift of these temperature boundaries can be affected either by the heat transfer rate produced by the synthesis reaction or by nonisothermal crystallization, upon quenching of the synthesis bath to ambient temperature. Thus, for nascent reactor powders, annealing effects, typical of different temperature regions likely superimpose, and the interpretation of dimensional changes and mass transfer on processing becomes less straightforward.

Such a superposition is confirmed by the annealing of reactor powders at 80 °C, which intermixes effects typical of the above described three temperature regions. In fact a general reduction of globular dimensions is the main result of this treatment, with samples synthesized at 30 °C showing a more significant decrease in the largest globules. Special consideration must be given to changes in the S185 samples. Tables 3 and 4 show that the largest group, R_5, disappears even for low-temperature treatment. Thickening of this globular radius above 600 Å, which is about the instrumental limit, should be excluded for an annealing temperature of 80 °C. However, the macroporosity of nascent powders[22,23] might suggest a different interpretation: according to the Babinet principle of reciprocity, the fifth dimensional group can correspond to large pores typical of the S185 morphologies (Figure 2). The largest group would then disappear as a consequence of the reduction of interparticle voids. This hypothesis has been discarded, because the R_5 group in the S185 samples has highly constant dimensional features, which do not agree with the random distribution of pore sizes reported for nascent systems.[22,23] These constant features of the largest nascent dimensional group are confirmed by both the R_5 multiplicity with respect to smaller dimensions and the constant values of R_5 for all the S185 samples (Table 2).

Disappearance of the R_5 group might be also related to increasing interparticle interference, causing a decrease in the scattered intensities at low angles.[38] This effect may become important as a consequence of the higher degree of compaction of the sintered samples. However, no significant dropping of intensities at low angles can be detected (Figure 4). At the same time, the significant increases in the mass fractions of the R_3 and R_4 dimensional groups suggest that the largest group in the S185 samples is highly unstable. Likely, binding forces are not strong enough to prevent these multiglobular aggregates from splitting into smaller

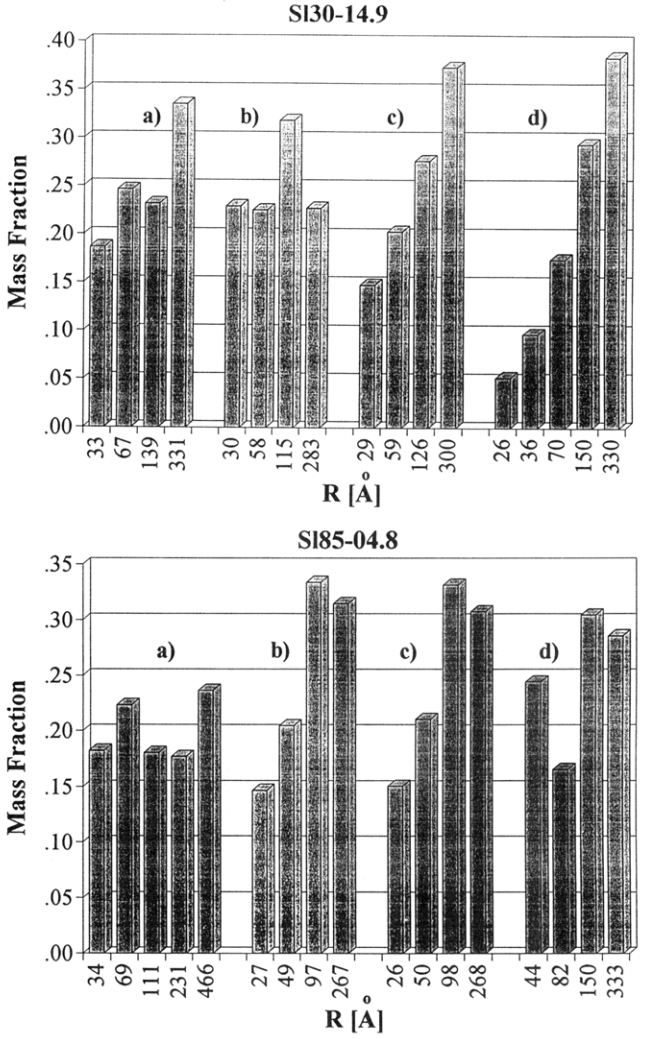

Figure 6. Effects of annealing on Guinier radii and mass fractions of dimensional groups of two samples obtained by different synthesis conditions: (a) nascent powder; (b) powder annealed for 15 days at 80 °C; (c) powder annealed for 32 days at 80 °C; (d) powder annealed for 32 days at 120 °C.

units as a consequence of dimensional rearrangements induced by annealing.

The shrinkage of the globular particles upon annealing at low temperature seems to be in contrast with several observations, reporting that crystallite thickening is the most common behavior on annealing. However, contributions from different simultaneous processes should be considered. Previous studies on the annealing of melt-crystallized PE[46] showed that crystal thickening involves dimensional changes in both the amorphous and the crystalline phase. If the annealing is above the crystallization temperature, an increase in the thickness of the crystalline lamellae and a simultaneous reduction of the noncrystalline phase is observed, after the system has been cooled to ambient. According to these observations, the decrease in R_i values can be explained by an extensive reduction of the noncrystalline phase, which is not completely compensated by the corresponding increase in the lamellar thickness.[46] This process is typical of the intermediate and high annealing temperature regions, but it may also apply to annealing at 80 °C. In fact inspection of data in Table 3 shows that some mass transfer from smaller to larger dimensional groups takes place even at 80 °C and, as reported in Figure 6, this leads to narrower size distributions.

A second contribution to the volume contractions observed on these annealed reactor powders stems from processes typical of the lower temperature region such as reductions of the crystalline defects associated with the fold surface imperfections, which more readily develop at higher undercoolings.[18] Defects may be also located inside the crystalline lattice, as a product of mechanical deformations on synthesis. Evidence of crystal lattice distortions in nascent powders is provided by the presence of monoclinic crystals, whose amount becomes more significant as the synthesis temperature is lowered.[10,47] Solid state transition from orthorombic to monoclinic crystals is obtained by deforming polyethylene samples along the orthorombic (110) plane, which converts to the monoclinic (010) plane.[48] The volume of the monoclinic unit cell is slightly larger than the orthorhombic one. Thus conversion from monoclinic to orthorhombic leads to a slight reduction of the crystalline portion of the globule. An additional contribution to shrinkage is provided by the elimination of the crystalline defects associated with the interface between the two different crystalline phases.[48] Since such a crystal-to-crystal conversion takes place above 60 °C, its effects should be particularly evident in samples annealed at 80 °C. In fact this temperature is low enough to enhance effects of monoclinic to orthorhombic conversion over crystal annealing. This is confirmed by data in Table 3: after annealing at 80 °C larger percent reduction in R_5 and more important mass transfer among different groups can be obtained in samples synthesized at 30 °C. These samples have a significant amount of the monoclinic form, compared to samples synthesized at higher temperatures, where the nascent content of monoclinic crystals is negligible.[10] It can also be noted that chain motions involved in these rearrangements at low temperature take place over long periods of time. A definite kinetic effect can be observed by comparing data on annealing for 15 and 32 days at 80 °C.

At 120 °C changes in the reactor powders follow undoubtedly the path of the annealing in the high-temperature region. A generalized increase in the values of radii for all the dimensional groups is coupled to significant increases in the weight fractions of the larger groups. This indicates that on sintering and annealing at high temperatures partial melting and recrystallization give an important contribution to crystallite thickening. R_i values of samples annealed at 120 °C support the model of thickening by preferred doubling. Data in Table 3 show that after annealing the dimensional multiplicity of most samples is better defined. In addition to this generalized behavior, some peculiarities related to synthesis conditions can be distinguished. Annealing and sintering induce more significant changes in radial dimensions and weight fractions of samples synthesized at higher temperatures. In fact S130 and Gp30 samples show comparatively smaller increases in the values of R_5 and wt % (R_5). Nascent differences in R_i values are greatly reduced by these thermal treatments.

Upon sintering, dimensions of R_i groups become quite similar and multiplicity becomes less distinct. These effects can be related to a reduction of sample microporosity. However the mass distribution profiles are rather different: in samples synthesized at low temperatures the largest weight fraction corresponds to the highest dimensional group. In contrast most of the other samples show the largest weight fraction in the dimensional group adjacent to the highest one. This feature may be a consequence of higher chain mobility in samples synthesized at higher temperatures. In S185 samples the complete reorganization of the nascent fifth dimensional group into different groups is also coupled with larger changes in radial dimensions and weight fractions.

A final observation is provided by the lack of any long distance interference peak in the SAXS patterns of sintered and annealed samples. These treatments do not modify the sample globular morphology, so that a regular lamellar organization is still missing after the first stage of the solid state processing.

Conclusions

Analysis of SAXS profiles of HMWPE nascent reactor powders by the generalized Guinier approximation have led us to conclude that these samples are organized in dimensional groups of globular particles. This conclusion agrees with SEM (Figure 2 and ref 26 and 27) and X-ray microtomography measurements[22,23] which show that clustering of small polymeric particles is a distinctive feature of nascent reactor powders. Globular aggregates of different sizes have been identified. The experimental profiles of nascent powders were found to be consistent with the scattering by a maximum of five dimensional groups. Two types of relationships between the nascent mesoscopic structures and the synthesis conditions have been obtained. Slurry polymerization at a high temperature (85 °C) packs larger amounts of nascent polymer into the bigger globules. As reported in Table 2 and Figure 4, the cumulative weight fractions of globules with diameters <100 Å are higher for samples synthesized at a low temperature (30 °C) and in the gas phase. This result agrees with measures of the melting peak breadths obtained by DSC:[9] both techniques lead to the conclusion that S185 samples have lower amounts of smaller crystallites.

Examination of the size of the globular aggregates in Table 2 provides a second correlation with synthesis conditions. S185 samples display R_i values which are quasi-multiples of 25 Å, up to the top value of 450 Å of the R_5 group. Such a multiplicity can be attributed to the clustering of small subunits into larger particles. Alternatively, annealing on synthesis can induced thickening of some portions of the nascent lamellar crystals. Preferred doubling of the initial fold length will then lead to a distribution of crystal dimensions, all approximate multiples of the original value. Models of the crystallization on synthesis at high temperatures support this explanation. However, this hypothesis cannot be confirmed by analysis of the SAXS profiles: void scattering likely obliterates effects related to the inner structure of the globular aggregates.

Both long time annealing and sintering at elevated temperatures do not destroy the globular morphology. SAXS patterns on reactor powders annealed for prolonged times do not show any evidence of a regular lamellar stacking. A melt crystallization step of the nascent powders is required to obtain the interferential peak, related to the regular stacking of crystalline and noncrystalline layers. On comparison, SAXS interference peaks are normally obtained from bulk-crystallized samples. This means that, for these samples, the superstructural organization, given by a regular lamellar stacking, is present from the first step of the solid state processing route. However, the absence of such a regular organization in reactor powders does not seem

to limit their ductilities, especially when the S185 samples are considered.

Polymer drawing has been thought to proceed by extension of a transient network, whose junctions are entanglements.[6,7,15] Accordingly, substantial improvements in ductility are expected from polymeric systems with low degrees of entanglements. It was suggested that crytallization on synthesis may provide less entangled morphologies.[2] This process does not require previous melting of long polymer chains, a step which would favor formation of entanglements. Investigations have focused on parameters which can estimate the nascent entanglement content. As reported in Figure 1, the good correlation between values of TDR_{max} and reactor powder crystallinities suggests that this last parameter is related to the entanglement degree. On crystallization, entanglements are excluded from the growing crystalline body and concentrate in the amorphous regions and in the interphase. At the same time, chain mobility is reduced by effect of the increasing entanglement density and crystallite growth is slowed. Thus, higher degrees of entanglements should correspond to lower crystallinities and larger amounts of smaller crystallites. Also the interphase thickness should be related to the entanglement density.[8,21] These three correlations have been experimentally verified. Higher values of TDR_{max} correspond actually to higher nascent crystallinities, lower interphase content[8] and lower amounts of small crystallites.[9]

Since entanglements are presumed to control chain mobility, investigations on the changes induced by sintering ((b) samples) and annealing ((c)-samples) can provide further information on the relationships between synthesis and drawability. Data obtained from SAXS patterns of annealed and sintered powders agree with data and models on the annealing of single crystals and melt-crystallized samples as reported.[45] However, the reactor powders examined in this work were crystallized directly on synthesis at high undercoolings. In this case sintering produces effects similar to those obtained by annealing above the crystallization temperature. In fact recrystallization of the smaller aggregates can be detected even at annealing temperatures as low as 8 °C, as shown by changes in weight fractions reported in Table 3 and Figure 4.

Conversion of the nascent monoclinic crystals to orthorhombic is another important effect of sintering, especially for samples synthesized at 30 °C, which have higher monoclinic contents. Investigations on nascent samples have not yet resolved ambiguities regarding the type of process which leads to crystallization into the monoclinic system. It has been reported that monoclinic crystals can be produced by crystal deformation stemming from the impingement of growing crystallites.[4,12] However, at high undercoolings, also the dynamics of the chain deposition on the crystal surface may favor the monoclinic form, by providing more space for the lateral packing of the adjacent chain segments. Small changes in the mesoscopic structure related to this crystal/crystal transition can be detected from the analysis of the SAXS patterns of samples annealed at 80 °C. Samples synthesized at 30 °C show larger volume reductions and more significant changes in the mass fraction of the globular aggregates after annealing at low temperatures.

As reported in Table 4 the most important effect of sintering is to reduce differences stemming from synthesis conditions. Similarities among the radii and the weight fractions of different samples are increased. No interference effect is detected, which leads us to conclude that sintering does not significantly improve the regularity in the stacking of nascent crystalline lamellae. SAXS patterns of sintered specimens do not provide significant correlations with sample ductilities. In contrast, as reported in Table 1, drawability of sintered samples depends strongly on synthesis conditions.

Estimates of the changes in the mesoscopic structure related to segmental chain mobility can be obtained by comparing differences between nascent and sintered samples. In this respect, the S185 samples display the most significant changes in radial dimensions and weight fractions coupled with the complete reorganization of the nascent largest dimensional group into different groups. The conclusion that these samples have higher chain mobility agrees with the hypothesis that such a higher mobility is a consequence of less-entangled nascent morphologies. Another confirmation is provided by the higher ductility of these samples, as measured by values of TDR_{max} reported in Table 1.

Gaussian analysis of SAXS profiles by the generalized Guinier approximation provides an adequate method for the characterization of nascent reactor powders. Several relationships between the mesoscopic structure of nascent specimens and synthesis conditions have been identified. In contrast, correlations with powder ductilities are less evident. Quite likely the structural changes in the first two stages of the solid state drawing procedure do not involve important and extensive variations of the chain arrangements which can directly affect ductility. SAXS investigations on coextruded morphologies should not suffer from these limits. The structural changes associated with coextrusion are much more important than those produced by sintering. Thus differences in the nascent features are enhanced by coextrusion, provided that chain rearrangements do not extend to the point of erasing the nascent morphologies. Under these conditions, it should be possible to extend the relationships between synthesis and structure to include also correlations with powder ductility, as shown here.

Acknowledgment. This work was partially supported by CNR, Progetto Strategico "Tecnologie Chimiche Innovative" and by Ministero per l'Universitá e la Ricerca Scientifica e Tecnologica (MURST). The authors also express appreciation to Union Carbide Corp., in particular to Dr. B. Wagner, for the samples and their characterization.

References and Notes

(1) Kanamoto, T.; Tsuruta, A.; Tanaka, K.; Takeda, M.; Porter, R. S. *Polym. J.* **1983**, *15*, 327.
(2) Zachariades, A. E.; Watts, M. P. C.; Kanamoto, T.; Porter, R. S. *J. Polym. Sci., Polym. Lett. Ed.* **1979**, *17*, 485.
(3) Kanamoto, T.; Ohama, T.; Tanaka, K.; Takeda, M.; Porter, R. S. *Polymer* **1987**, *28*, 1517.
(4) Smith, P.; Chanzy, H. D.; Rotzinger, B. P. *J. Mater. Sci.* **1987**, *22*, 523.
(5) Wang, L. H.; Ottani, S.; Porter, R. S. *Polymer*. **1991**, *32*, 1776.
(6) Smith, P.; Lemstra, P. J. *Colloid Polym. Sci.* **1980**, *258*, 891.
(7) Smith, P.; Lemstra, P. J.; Booij, H. C. *J. Polym. Sci., Polym. Phys. Ed.* **1981**, *19*, 877.
(8) Wang, L. H.; Porter, R. S.; Stidham, H. D.; Hsu, S. L. *Macromolecules* **1991**, *24*, 5535.
(9) Ottani, S.; Porter, R. S. *J. Polym. Sci., Part B: Polym. Phys.* **1991**, *29*, 1179.
(10) Ottani, S.; Porter, R. S. *Polymer* **1990**, *31*, 369.
(11) Wang, L. H.; Ottani, S.; Porter, R. S. *J. Polym. Sci., Part B: Polym. Phys.* **1991**, *29*, 1189.

(12) Chanzy, H. D.; Day, A.; Marchessault, R. H. *Polymer* **1967**, *8*, 567.
(13) Chanzy, H. D.; Revol, J. F.; Marchessault, R. H.; Lamandé, A. *Kolloid Z. Z. Polym.* **1972**, *251*, 563.
(14) Wunderlich, B.; Comier, C. H. *J. Polym. Sci., Polym. Phys. Ed.* **1967**, *5*, 987.
(15) Graessley, W. W. *Adv. Polym. Sci.* **1974**, *16*, 4.
(16) Mehta, A.; Wunderlich, B. *Makromol. Chem.* **1974**, *175*, 977.
(17) DiMarzio, E. A.; Guttman, C. M.; Hoffman, J. D. *Faraday Discuss. Chem. Soc.* **1979**, *68*, 210.
(18) Hoffman, J. D. *Polymer* **1983**, *24*, 3.
(19) Wunderlich, B. *Macromolecular Physics*; Academic Press: New York, 1976; Vol. 2.
(20) Munoz-Escalona, A.; Parada, A. *Polymer* **1979**, *20*, 859.
(21) Strobl, G. R.; Hagedorn, W. *J. Polym. Sci., Polym. Phys. Ed.* **1979**, *16*, 1181.
(22) Conner, W. C.; Webb, S. W.; Spanne, P.; Jones, K. W. *Macromolecules* **1990**, *23*, 4742.
(23) Ferrero, M. A.; Sommer, R.; Spanne, P.; Jones, K. W.; Conner, W. C. *J. Polym. Sci., Part A: Polym. Chem.* **1993**, *31*, 2507.
(24) Munoz-Escalona, A.; Villamizar, C.; Frias, P. In Structure and Morphology of Nascent Polyethylenes Obtained by TiCl Heterogeneous Ziegler–Natta Catalysts. *Structure Property Relationships of Polymeric Solids*; Hiltner, Anne, Ed.; Plenum Press: New York, 1983.
(25) Nooijen, G. A. H. *Eur. Polym. J.* **1994**, *30*, 11.
(26) Bailly, J. C.; Hagege, R. *Polymer* **1991**, *32*, 181.
(27) Hagege, R.; Bailly, J. C. *Polymer.* **1993**, *34*, 2720.
(28) Vonk, C. G. *J. Appl. Crystallogr.* **1971**, *4*, 340.
(29) Geil, H. P. *Polymer Single Crystals*; Interscience Publishers, John Wiley: New York, 1963.
(30) Mandelkern, L. *Crystallization of Polymers*; McGraw-Hill: New York, 1964.
(31) Peterlin, A. *J. Polym. Sci., Part C* **1965**, *9*, 1.
(32) Tervoort-Engelen, Y. M. T.; Lemstra, P. J. *Polym. Commun.* **1991**, *32*, 343.
(33) Brady, J. M.; Thomas, E. L. *Polymer* **1989**, *30*, 1615.
(34) Hosemann, R.; Hentschell, M.; Ferracini, E.; Ferrero, A.; Martelli, S.; Riva, F.; Vittori Antisari, M. *Polymer* **1982**, *23*, 979.
(35) Hosemann, R.; Bagchi, S. N. *Direct Analysis of Diffraction by Matter*; North-Holland Publishing Co.: Amsterdam, 1962.
(36) Klug, L. P.; Alexander, L. E. *X-ray Diffraction Procedures for Polycrystalline and Amorphous Materials*; John Wiley: New York, 1974.
(37) Joerchel, O. *Z. Naturforsch.* **1957**, *12A*, 123.
(38) Durchschlag, H. *Biophys. Struct. Mech.* **1975**, *1*, 153.
(39) Bonart, R. *Kolloid Z. Z. Polym.* **1964**, *194*, 97.
(40) Vonk, C. G. *J. Appl. Crystallogr.* **1975**, *8*, 340.
(41) Guinier, A.; Fournet, G. *Small Angle Scattering of X-rays*; John Wiley: New York, 1955.
(42) (a) Wunderlich, B. *Macromolecules Physics*; Academic Press: New York, 1976; Vol. 2, pp 354–357. (b) Burmester, A. F.; Dreyfuss, P.; Geil, P.; Keller, A. *J. Polym. Sci., Polym. Lett. Ed.* **1972**, *10*, 769. (c) Dreyfuss, P.; Keller, A. *J. Polym. Sci., Part B* **1970**, *8*, 253.
(43) Wunderlich, B. *Macromolecular Physics*; Academic Press: New York, 1976; Vol. 2, pp 282–293.
(44) Vonk, C. G. *J. Appl. Crystallogr.* **1976**, *9*, 433.
(45) Wunderlich, B. *Macromolecular Physics*; Academic Press: New York, 1976; Vol. 2, pp 374–394. See the references in the text and at the end of the chapter for an extensive bibliography on this matter.
(46) Kavesh, S.; Schultz, J. M. *J. Polym. Sci., Polym. Phys. Ed.* **1971**, *9*, 85.
(47) Jarrett, W. L.; Mathias, L. J.; Porter, R. S. *Macromolecules* **1990**, *23*, 5164.
(48) Takahashi, Y.; Ishida, T. *J. Polym. Sci., Part B: Polym. Phys.* **1988**, *26*, 2267.

MA9450344